

1           **A program to analyse optical coherence tomography images of the ciliary muscle**

2           Deborah S. Laughton<sup>1</sup>, Benjamin J. Coldrick<sup>1,2</sup>, Amy L. Sheppard<sup>1</sup> & Leon N. Davies<sup>1</sup>

3           <sup>1</sup>Ophthalmic Research Group, Life & Health Sciences, Aston University, Birmingham, UK

4           <sup>2</sup>Biomedical Engineering, Life & Health Sciences, Aston University, Birmingham, UK

5

6           **Corresponding author**

7           Leon N Davies PhD, Ophthalmic Research Group, Life & Health Sciences, Aston University,

8           Birmingham, B4 7ET, UK

9           Tel: +44(0)121 204 4152

10          Fax: +44 (0) 121 204 4048

11

12          **Keywords:** Accommodation, AS-OCT, ciliary muscle, presbyopia

13

14          **Disclosure:** The authors report no conflicts of interest and have no proprietary interest in any of the  
15          materials mentioned in this article

16          **Acknowledgments:** DL is supported by a College of Optometrists Postgraduate Research Scholarship.  
17          We would like to acknowledge Ms Naomi Richa Saigal for imaging the rigid gas-permeable lenses.

18

19

20

21 **Abstract**

22 **Purpose**

23 To describe and validate bespoke software designed to extract morphometric data from ciliary  
24 muscle Visante Anterior Segment Optical Coherence Tomography (AS-OCT) images.

25 **Method**

26 Initially, to ensure the software was capable of appropriately applying tiered refractive index  
27 corrections and accurately measuring orthogonal and oblique parameters, 5 sets of custom-made  
28 rigid gas-permeable lenses aligned to simulate the sclera and ciliary muscle were imaged by the  
29 Visante AS-OCT and were analysed by the software. Human temporal ciliary muscle data from 50  
30 participants extracted via the internal Visante AS-OCT caliper method and the software were  
31 compared. The repeatability of the software was also investigated by imaging the temporal ciliary  
32 muscle of 10 participants on 2 occasions.

33 **Results**

34 The mean difference between the software and the absolute thickness measurements of the rigid  
35 gas-permeable lenses were not statistically significantly different from 0 ( $t=-1.458$ ,  $p=0.151$ ). Good  
36 correspondence was observed between human ciliary muscle measurements obtained by the  
37 software and the internal Visante AS-OCT calipers (maximum thickness  $t=-0.864$ ,  $p=0.392$ , total  
38 length  $t=0.860$ ,  $p=0.394$ ). The software extracted highly repeatable ciliary muscle measurements  
39 (variability  $\leq 6\%$  of mean value).

40 **Conclusion**

41 The bespoke software is capable of extracting accurate and repeatable ciliary muscle measurements  
42 and is suitable for analysing large data sets.

43

44

45

46 **Introduction**

47 Despite the involvement of the ciliary muscle in accommodation [1-3], presbyopia [4-5], and possibly  
48 myopia development [6-9], there is a relative paucity of *in vivo* ciliary muscle research. Indeed,  
49 imaging the ciliary muscle *in vivo* represents a significant challenge due to the obscured position of  
50 the ciliary muscle behind the highly pigmented iris.

51 Traditionally, ultrasound biomicroscopy (UBM) has been utilised to acquire *in vivo* images of the  
52 ciliary muscle [10-13]. However, sharper image definition obtained with Anterior Segment Optical  
53 Coherence Tomography (AS-OCT) permits superior localisation of the scleral spur (a key reference  
54 point for ciliary muscle measurements), compared to UBM images [13]. The axial resolution is 8  $\mu\text{m}$   
55 and 25  $\mu\text{m}$  for the Visante AS-OCT (Carl Zeiss Meditec, California, USA) in high resolution corneal  
56 mode and the P40 UBM (Paradigm Medical Industries, Utah, USA) at 50 MHz [13], respectively.  
57 Additionally, UBM necessitates supine posture, topical anaesthetic, coupling agents and  
58 contralateral eye fixation, whereas the Visante AS-OCT permits non-contact ipsilateral imaging of the  
59 fixating eye whilst the patient is sitting up-right, which affords enhanced patient comfort and  
60 feasibly permits paediatric assessment [2,6]. Therefore more recent research has progressed to use  
61 AS-OCT devices rather than UBM to image the ciliary muscle *in vivo* [1-6, 8-9].

62 Similarly to UBM devices, in-built Visante AS-OCT software allows calipers to be super-imposed onto  
63 acquired images to extract measurements. During image analysis, the Visante AS-OCT internal  
64 software outlines the boundaries of the ocular media and applies corrective refractive indices ( $n$ ) to  
65 improve measurement accuracy ( $n=1.000$  anterior to the cornea,  $n=1.338$  to the cornea,  $n=1.343$   
66 posterior to the cornea). However, the Visante AS-OCT also fits the same refractive index  
67 adjustments to ciliary muscle images, with no option to alter the magnitude of the tiered refractive  
68 index corrections. Therefore, previous authors have applied a refractive index of 1.000 to the entire  
69 ciliary muscle image [1,4,6]. To provide data more closely associated with physiological *in vivo* ciliary  
70 muscle parameters, Sheppard and Davies [1,4] adjusted their ciliary muscle caliper measurements to

71 account for a refractive index of 1.382, which is the best estimate of the refractive index of the  
72 ciliary muscle based on *in vitro* bovine muscle tissue studies using confocal microscopy [14] and *in*  
73 *vitro* human ventricular muscle studies using OCT [15]. However, the refractive indices of the  
74 overlying sclera, as well as the ciliary muscle itself, need to be compensated for to ensure the  
75 magnitude of the measured ciliary muscle parameters are as accurate as possible. Furthermore, the  
76 ciliary muscle tissue is not accurately represented by the straight lines of the calipers because the  
77 scleral and ciliary muscle tissues are curved, to varying degrees in different patients [16]. Therefore,  
78 to improve the accuracy of morphological assessment, data have been exported for analysis with  
79 external software [16].

80 Due to the lack of uniformity of the ciliary muscle outline in Visante AS-OCT images, Kao and  
81 colleagues' [16] software required manual localisation of the scleral spur before automated image  
82 analysis commenced. Once the sclera and ciliary muscle had been outlined, refractive indices of 1.41  
83 and 1.38 were applied across the y-axis of the scleral and ciliary muscle image sections, respectively.  
84 The software produced vertical thickness measures at 1, 2 and 3 mm behind the scleral spur,  
85 maximum thickness and measured the cross-sectional area of the anterior ciliary body. However, the  
86 edge detection algorithms appeared to incorporate both the ciliary muscle and the pigmented ciliary  
87 epithelium, which may overestimate ciliary muscle measurements. Furthermore, measurements of  
88 ciliary muscle length were not obtained.

89 Despite the Visante AS-OCT's use in previous morphometric studies of the ciliary muscle, the  
90 instrument remains susceptible to optical and instrument distortions, and has limited inbuilt  
91 capabilities to quantify ciliary muscle parameters. Consequently, to overcome the limitations of  
92 previously designed software [16] and to address concerns of the subjectivity of identifying the  
93 posterior end point of the ciliary muscle [17], bespoke software was developed. The aim of this  
94 study was to describe and validate the bespoke software and to compare data extracted by the  
95 software and the internal Visante AS-OCT calipers.

96 **Method**

97 The study was approved by the Aston University Research Ethics Committee and was conducted in  
98 accordance with the tenets of the Declaration of Helsinki. Informed consent was obtained from all  
99 participants after explanation of the nature and possible consequences of the study. One UK  
100 registered optometrist (DL) acquired and extracted all the human data.

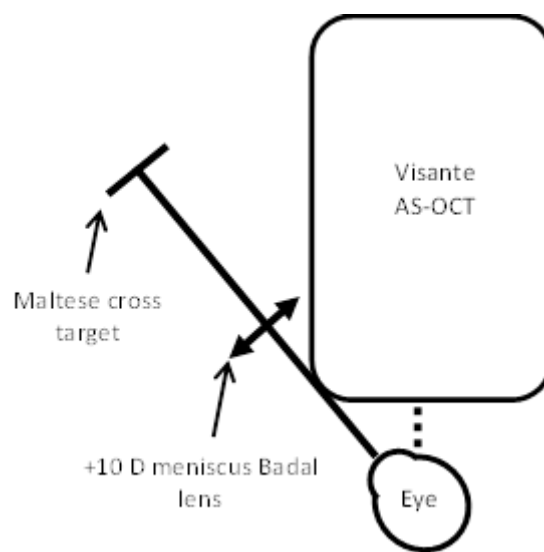
101 ***Ciliary muscle image acquisition***

102 It is likely that the repeatability of nasal ciliary muscle image analysis is superior to temporal ciliary  
103 muscle image analysis because the scleral spur is more easily discernible nasally [18], therefore only  
104 temporal ciliary muscle images were analysed in the present study.

105 Each participant wore an eye patch over their left eye throughout data collection. Participants were  
106 asked to place their chin and forehead against the Visante AS-OCT supports and fixate straight-  
107 ahead at the centre of the internal star target. The chin rest was adjusted to align the participant's  
108 right eye to allow visualisation of the anterior crystalline lens surface, which was guided by the real-  
109 time Visante AS-OCT video stream of the external eye. High resolution corneal mode was selected  
110 (scanning an area of 10 mm in width and 3 mm in depth) and participants were aligned to ensure the  
111 vertical white fixation line was visible through the centre of the image, which indicated the  
112 measurement beam was coincident with the optical axis of the eye [19].

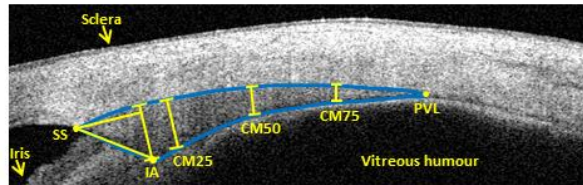
113 In order to image the full length of the ciliary muscle using the Visante AS-OCT, patients must avert  
114 their gaze to a point external to the central viewing window because the iris blocks visualisation of  
115 the ciliary muscle in primary gaze. Fig. 1 illustrates the bespoke Badal lens system with a moveable  
116 Maltese cross target, attached to the forehead rest of the Visante AS-OCT to provide a steady  
117 peripheral fixation target and to correct for ametropia. The minimum level of horizontal eye  
118 movement required to ensure the peripheral target is unobstructed by the instrument casing is 40°  
119 from the internal Visante AS-OCT star target. Fixating externally causes the Visante AS-OCT beam to

120 be directed through the sclera, rather than the cornea, reducing optical distortion due to the flatter  
121 scleral plane. Since all participants were aligned to the optical axis of the Visante AS-OCT in primary  
122 position, only minor vertical alignment adjustments were required once the participant adducted  
123 their right eye to view the centre of the external Maltese cross. Horizontal alignment was  
124 determined by the real-time Visante AS-OCT video stream of the OCT image, which was adjusted to  
125 ensure simultaneous visualisation of the scleral spur and ciliary muscle posterior visible limit, as  
126 depicted in Fig. 2.



127

128 **Fig. 1.** Schematic diagram of the Visante AS-OCT with bespoke Badal lens system attachment. The  
129 dashed line represents the path of the OCT beam through the sclera. The Maltese cross target is  
130 positioned 10 cm from the Badal lens in order to stimulate 0.00 D of accommodation in an  
131 emmetropic patient.



132

133 **Fig. 2.** Visante AS-OCT image of a human ciliary muscle section. The ciliary muscle is outlined in blue  
 134 with superimposed yellow caliper measurements. PVL = posterior visible limit; SS = scleral spur; IA =  
 135 inner apex; CM25, CM50, CM75 = thickness at 25%, 50% and 75% of curved total length (SS to PVL);  
 136 maximum thickness = perpendicular distance from IA to sclera; anterior length = perpendicular  
 137 distance from line of maximum thickness to SS. The pigmented epithelium is visible underneath the  
 138 inner apex and the inferior ciliary muscle border.

139 Once accurately aligned, the Maltese cross target was moved to provide a 0.00 D accommodative  
 140 stimulus for each participant. Participants were asked to focus on the centre of the Maltese cross  
 141 target and keep it as clear as possible throughout data collection, whilst also keeping their head and  
 142 eyes as still as possible. Three consecutive images of the right eye temporal ciliary muscle were  
 143 acquired and saved.

144 **Software design**

145 The preparation of ciliary muscle images for analysis was similar to the process used by Kao *et al.*  
146 [16]; all images acquired in high resolution corneal mode were exported in raw DICOM (Digital  
147 Imaging and Communications in Medicine) form (n=1.00) and were imported to Matlab R2012b (The  
148 MathWorks Inc., Massachusetts, USA) and subsequently resized to 512 x 1280 pixels, matching the  
149 correct aspect ratio. The images were not cropped or reduced in size for processing.

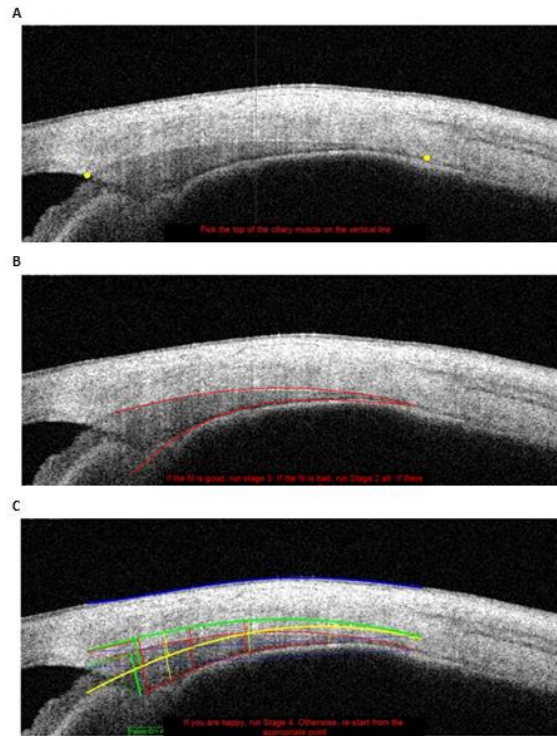
150 Due to the difficulties in localising the outline of the ciliary muscle, the bespoke software required  
151 multiple landmarks to be manually selected before extracting data. Initially, the scleral spur and a  
152 point beyond the posterior visible limit were selected manually (highlighted by yellow dots in Fig.  
153 3A). The software then calculates the distance between these two markers and superimposes a  
154 vertical line midway, prompting the user to pick the points where the scleral/ciliary muscle and  
155 ciliary muscle/pigmented ciliary epithelium boundaries bisect the line. These initial steps identify the  
156 area of interest to the software, which then superimposes a block of 10 vertical lines spaced at 1  
157 pixel intervals every 0.5 mm between the scleral spur and posterior point chosen. The change in  
158 pixel intensity along each line is determined. To define the ciliary muscle border, a 2<sup>nd</sup> order Fourier  
159 series is fitted to the intensity profile and differentiated. The location of the largest peak formed in  
160 the differentiated intensity profile corresponds to the point where the line bisects the ciliary muscle  
161 boundary (the crossing point). This process is repeated for the top and bottom of each line  
162 separately in order to determine crossing points of both the superior and inferior ciliary muscle  
163 boundaries on the OCT image. A 2<sup>nd</sup> order polynomial curve is fitted to the crossing points of each  
164 boundary.

165 The ciliary muscle/pigmented ciliary epithelium border is not as easily discriminated as the  
166 scleral/ciliary muscle border, therefore the software provides an option to manually pick three  
167 points along the boundary to improve the fit of the curve, if the automated fit is not satisfactory (Fig.  
168 3B). Due to relatively poor image clarity around the inner apex of the ciliary muscle, the inner apex

169 must also be selected manually. Once the fit of the curves to the ciliary muscle borders has been  
170 finalised, the OCT image is converted to a binary image in order for internal MatLab edge detection  
171 algorithms to identify the air/scleral boundary and fit a 2<sup>nd</sup> order polynomial curve to it. During  
172 software development and testing, it was determined that 2<sup>nd</sup> order curves accurately and  
173 satisfactorily fitted the contour of the ciliary muscle and sclera in all patients tested.

174 Subsequently, the software applies a tiered refractive index correction to the scleral and ciliary  
175 muscle tissue (1.41 and 1.38, respectively), as shown in Fig. 3C by the higher yellow and green  
176 curves. The posterior visible limit of the ciliary muscle is identified as the point where the curves  
177 fitted to the ciliary muscle borders reach minimum separation posteriorly. The software exports the  
178 Straight-line TL (straight-line distance between the scleral spur and posterior visible limit), Curved TL  
179 (ciliary muscle total length measured along the scleral/ciliary muscle boundary), Max T (maximum  
180 thickness; see Fig. 2), Ant L (anterior length measured perpendicularly from the line of maximum  
181 thickness to the scleral spur), SS-IA (distance between scleral spur to the inner apex), CM2 (thickness  
182 measured 2 mm from the scleral spur along the scleral curve), CM25 (thickness measured at 25% of  
183 the total curved length of the ciliary muscle), CM50 (thickness measured at 50% of the total curved  
184 length of the ciliary muscle) and CM75 (thickness measured at 75% of the total curved length of the  
185 ciliary muscle), directly to an Excel spreadsheet, allowing the examiner to be masked to the results.

186 Due to the uncertainties of measuring thickness at fixed distances from the scleral spur, which is  
187 likely to represent a different anatomical area of the ciliary muscle between subjects, CM1  
188 (thickness measured 1 mm behind the scleral spur along the scleral curve) and CM3 (thickness  
189 measured 3 mm behind the scleral spur along the scleral curve) were not quantified. However, CM2  
190 was included due to the hypothesis this area may act as a fulcrum point during accommodation,  
191 where the net change in thickness is negligible [2].



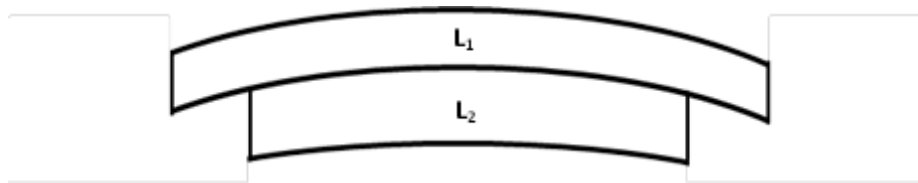
192

193 **Fig 3.** A) Screenshot from the software after the scleral spur and a point beyond the posterior visible  
 194 limit (yellow dots) have been clicked on. The user is required to select where the top and bottom  
 195 ciliary muscle boundaries are bisected by the superimposed vertical line. B) The software outlines  
 196 the boundaries of the ciliary muscle and gives the option to manually redefine the lower curve. C)  
 197 After manually selecting the inner apex the software extracts the ciliary muscle data, correcting for  
 198 the refractive indices of the sclera and ciliary muscle (higher yellow and green curves) and transfers  
 199 the data to an Excel document.

200 ***Software analysis of artificial ciliary muscle sections***

201 To ensure the software was capable of appropriately applying refractive index corrections and  
 202 accurately measuring orthogonal and oblique parameters, a series of custom-made rigid gas-  
 203 permeable lenses (No. 7 Contact Lens Laboratory Ltd, Hastings, UK) of known dimensions were  
 204 imaged by the Visante AS-OCT. One silicon-acrylate lens ( $n = 1.48$ ) simulated the sclera ( $L_1$  in Fig. 4)

205 and 5 fluoro-polymer lenses ( $n=1.44$ ) of varying thickness (0.3, 0.45, 0.6, 0.75, 0.9 mm) each  
206 simulated the ciliary muscle ( $L_2$  in Fig. 4). Each of the ciliary muscle lenses were of constant  
207 thickness. The total diameter of the sclera lens was 10 mm and each ciliary muscle lens was 6 mm.  
208 The radius of curvature of the lenses was 12 mm. A ciliary muscle lens and the sclera lens were  
209 positioned together, as shown in Fig. 4, for image acquisition. For each of the 5 ciliary muscle and  
210 sclera lens combinations, 10 OCT images were acquired and exported as raw data.



211

212 **Fig. 4.** Schematic diagram of two rigid gas-permeable lenses designed to simulate the sclera ( $L_1$ ) and  
213 the ciliary muscle ( $L_2$ ).

214 For this exercise only, the ciliary muscle software was adapted to allow 3 points across each of the  
215 lens boundaries to be manually selected for subsequent automated polynomial curve (order 2)  
216 fitting. The software determines the length of the ciliary muscle lens as the straight-line distance  
217 between the first and third points plotted across the scleral/ciliary muscle boundary, therefore the  
218 edges of the lens were manually selected. The thicknesses of the ciliary muscle lenses were  
219 measured at 25 (CM25), 50 (CM50) and 75% (CM75) across the lens diameter. Each thickness  
220 measurement was measured perpendicular to the scleral/ciliary muscle boundary curve. The  
221 refractive indices of the scleral and ciliary muscle lenses (1.48 and 1.44, respectively) were inputted  
222 to allow the program to compensate the measurements. All measurements were exported directly  
223 to an Excel spreadsheet, masking the examiner to the results during data extraction. The diameter  
224 and thickness measurements of the ciliary muscle lenses were also measured 10 times by Vernier  
225 calipers and compared to the results produced by the software.

226 The bias of the measurements was calculated from the mean difference between the two  
227 techniques. A paired t-test was used to determine whether the bias was significantly different from

228 0. The spread over which 95% of the data lie (limits of agreement, LoA) was calculated and the  
229 agreement of the software and Vernier calipers was analysed using a Bland-Altman plot [20].

### 230 ***Software and Visante AS-OCT caliper agreement***

231 Human ciliary muscle parameters acquired by the software were compared to those acquired via the  
232 traditional method of ciliary muscle Visante AS-OCT image analysis: internal Visante AS-OCT calipers.  
233 Disaccommodated temporal ciliary muscle images of 50 patients (mean age  $39.11 \pm 3.18$  years;  
234 mean spherical equivalent  $-1.17 \pm 2.09$  D, range  $-7.07$  to  $+0.49$  D; mean astigmatism  $-0.59 \pm 0.57$  D)  
235 were acquired and data were subsequently extracted by the software and the Visante AS-OCT  
236 calipers on separate occasions.

237 The software was designed to measure the ciliary muscle thickness with reference to the curved  
238 ciliary muscle length (following the contour of the scleral/ciliary muscle border), whereas the Visante  
239 AS-OCT calipers cut across the ciliary muscle to measure its thickness at horizontal distances from  
240 the scleral spur. Therefore, the calipers are likely to underestimate the thickness measurements in a  
241 more curved ciliary muscle [6,16]. Due to the aforementioned differences in the origin of thickness  
242 measurements from the scleral spur, only the Straight-line TL and Max T measurements were  
243 compared between the two methods. The software Straight-line TL and the software Curved TL  
244 values were also compared.

245 Internal Visante AS-OCT caliper measurements were acquired by applying a refractive index of 1.00  
246 to the entire image and superimposing calipers on to the ciliary muscle image to extract Straight-line  
247 TL and Max T measurements. For comparison with the internal Visante AS-OCT caliper  
248 measurements, the software was adapted to export the raw ciliary muscle measurements with a  
249 refractive index of 1.00 applied to the entire image.

250 The bias was calculated from the mean difference between the techniques and a paired t-test was  
251 used to determine whether the bias was significantly different from 0. The agreement of the

252 techniques was also analysed using Bland-Altman plots. The difference between the software  
253 Straight-line TL and the software Curved TL values was analysed using a paired t-test.

#### 254 ***Repeatability of software analysis of human ciliary muscle***

255 Additionally, the repeatability of human ciliary muscle OCT imaging and software interpretation was  
256 determined by inviting 10 participants to return for ciliary muscle imaging on a separate occasion,  
257 less than 1 week after their first appointment. A further three ciliary muscle images were acquired  
258 and analysed.

259 In order to determine the errors arising from patient alignment and software interpretation, the  
260 ciliary muscle of a single patient's right eye was imaged 10 times at 0.00 D accommodative stimulus  
261 during one appointment. The patient was asked to remove and reposition their chin and forehead  
262 between the acquisition of each image. In order to isolate the repeatability of the software  
263 interpretation and analysis of a ciliary muscle image, 1 image was analysed 10 times.

264 The bias of each parameter was calculated from the mean difference between visits. A paired t-test  
265 was used to determine whether the bias was significantly different from 0.

### 266 **Results**

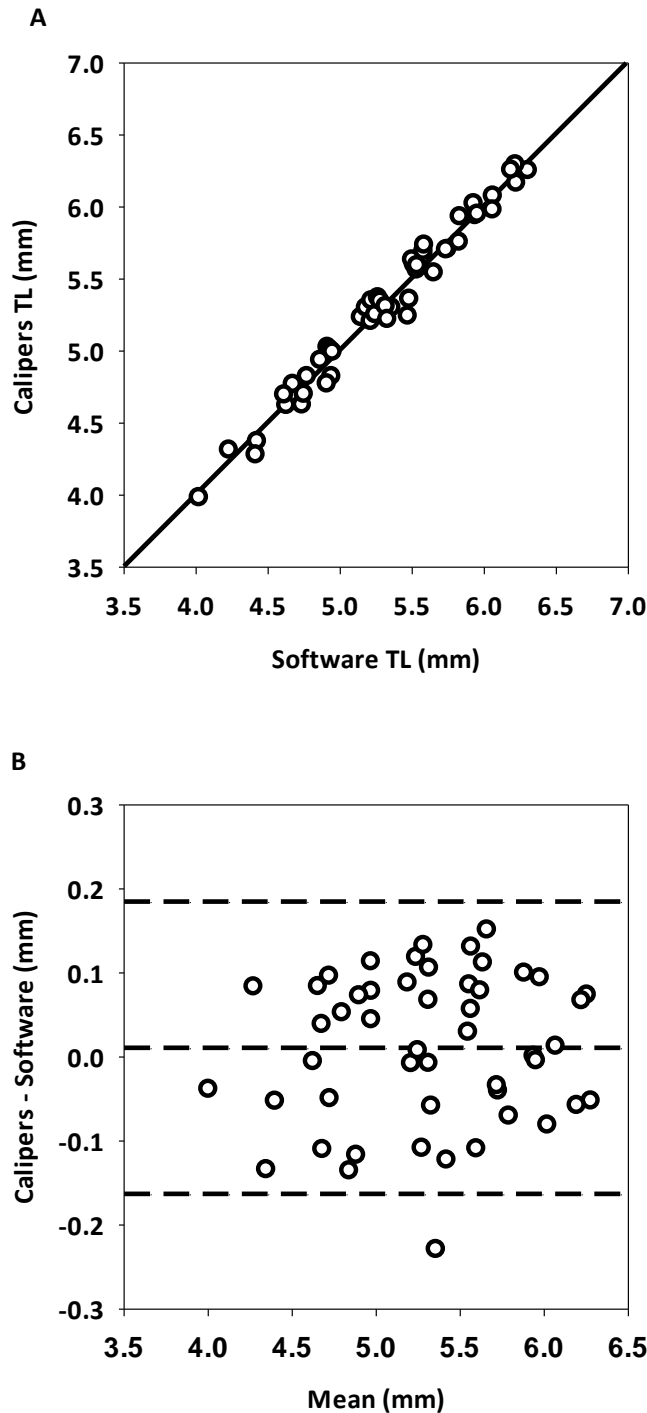
#### 267 ***Artificial ciliary muscle sections***

268 The mean difference between the software and the Vernier caliper measurements are displayed in  
269 Table 1. The bias of CM25, CM50 and CM75 were not significantly different from 0. The bias was not  
270 correlated with the magnitude of the measurement. However the total diameter was significantly  
271 underestimated by the software ( $p=0.001$ ).

#### 272 ***Software and caliper agreement***

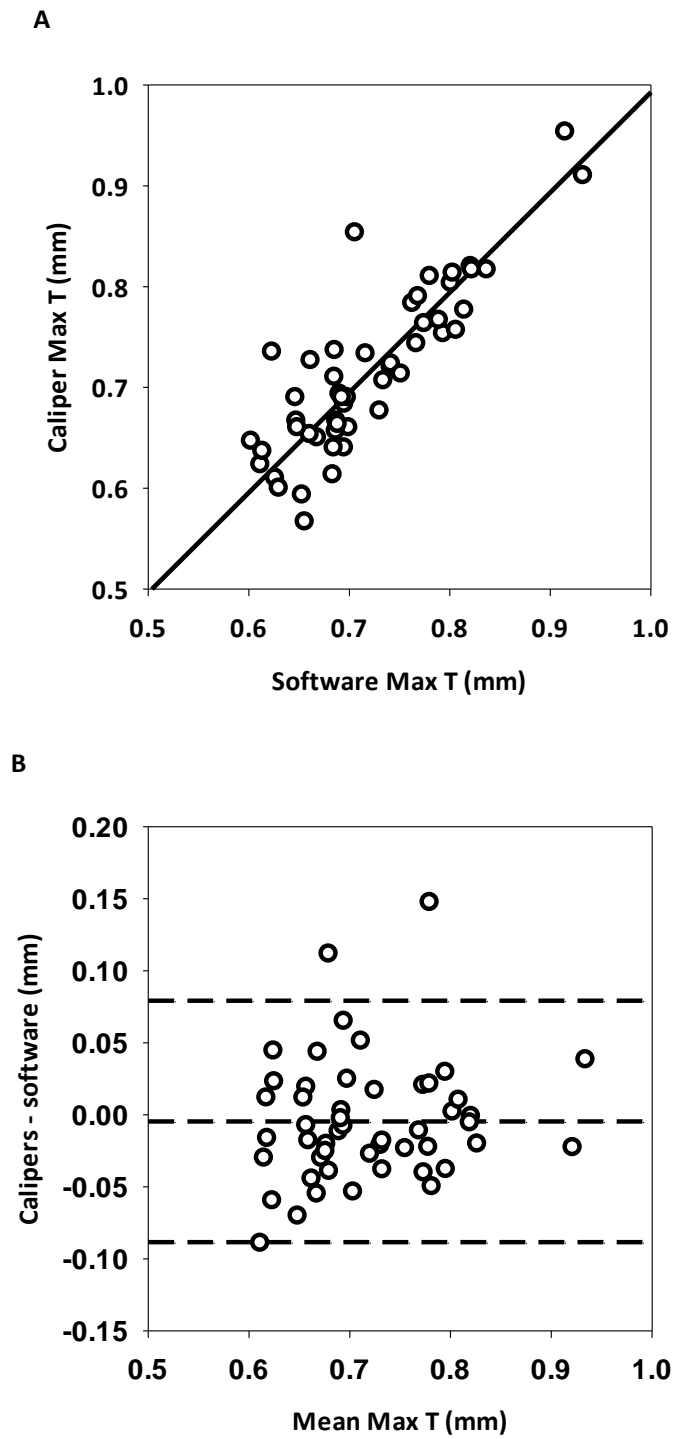
273 The mean difference between the software and the Visante AS-OCT internal caliper total Straight-  
274 line TL and Max T measurements are displayed in Table 2. The bias of each parameter was not  
275 significantly different from 0. The data are displayed graphically with Bland-Altman plots in Figs 5

276 and 6, which show the bias was not correlated to the magnitude of the measurement. The mean  
277 software Curved TL measurements ( $5.391 \pm 0.571$  mm) were significantly longer than the mean  
278 software Straight-line TL measurements ( $5.301 \pm 0.560$  mm;  $t=-23.356$ ,  $p<0.001$ ).



279  
280 **Fig. 5. A.** Total straight-line length measured by the software and the internal Visante AS-OCT  
281 calipers. Regression line  $y=0.132+0.973x$ ,  $R^2=0.876$ ,  $p<0.001$ . **B.** Bland-Altman plot of the agreement  
282 between total straight-line length measured by the software and the internal Visante AS-OCT

283 calipers. Regression line  $y=-0.068+0.015x$ ,  $R^2=0.009$ ,  $p=0.514$ . The dashed lines represent the limits  
284 of agreement.



285  
286 **Fig. 6. A** Maximum thickness measured by the software and the internal Visante AS-OCT calipers.  
287 Regression line  $y=0.152+0.794x$ ,  $R^2=0.732$ ,  $p<0.001$ . **B.** Bland-Altman difference versus mean plot of  
288 the agreement between maximum thickness measured by the software and the internal Visante AS-

289 OCT calipers. Regression line  $y=-0.063+0.081x$ ,  $R^2=0.021$ ,  $p=0.317$ . The dashed lines represent the  
290 limits of agreement.

291

### 292 **Repeatability**

293 The bias of ciliary muscle parameters measured in 10 patients across 2 visits is displayed in Table 3.  
294 The bias represented  $\leq 6\%$  of the mean value of each parameter and was not significantly different  
295 from 0. Tables 4 and 5 obtained from 1 patient realigned 10 times and 1 image analysed 10 times,  
296 respectively, suggest approximately 60% of the difference encountered between visits is likely to be  
297 due to the inherent variability associated with manually selecting points for analysis with the  
298 bespoke software.

### 299 **Discussion**

300 The software described here is capable of accurately outlining the ciliary muscle, applying  
301 appropriate refractive index corrections and extracting a variety of repeatable orthogonal and  
302 oblique ciliary muscle parameters, thus verifying its suitability for *in vivo* ciliary muscle analysis.  
303 Compared to the Visante AS-OCT calipers, the software enables more accurate measurements of the  
304 curved ciliary muscle tissue to be acquired by following the scleral/ciliary muscle contour, rather  
305 than cutting horizontally across the ciliary muscle to measure thicknesses with respect to the  
306 distance from scleral spur. Image analysis can also be performed remotely to the Visante AS-OCT  
307 device on an external computer. As with the Visante AS-OCT's calipers, the bespoke software is not  
308 fully automated and requires user input at various stages of the analysis.

309 The software raw parameters (n=1.00) compared favourably to internal Visante AS-OCT caliper  
310 Straight-line TL and Max T measurements, suggesting the location of the posterior visible limit,  
311 utilised in the total length measurement, is not only evident across a large sample of patients, but  
312 can also be consistently identified subjectively and objectively. Nevertheless, the concerns of  
313 previous authors over the visibility of the posterior end point of the ciliary muscle are not entirely

314 unfounded [17]; extensive analysis of ciliary muscle images during software development has shown  
315 there is large intersubject variability in the visibility of the posterior limit of the ciliary muscle. In  
316 order to simplify localisation for the software, the posterior visible limit was defined as the point  
317 where the scleral/ ciliary muscle and ciliary muscle/ pigmented ciliary epithelium contours reached  
318 minimum separation posteriorly, which produced highly repeatable results.

319 Orthogonal and oblique thickness measurement accuracy was evidenced by computation of the  
320 distance between 2 polynomial curves (order 2) fitted to OCT images of 2 superimposed rigid gas-  
321 permeable lenses. As expected, the total diameter measurements were significantly underestimated  
322 by the software ( $p=0.001$ ) due to difficulties ensuring the scleral and ciliary muscle lenses were  
323 perfectly centred, and that the measurement beam scanned across the centre of both lenses.  
324 Nonetheless, the validity of horizontal measurements has been confirmed by the good  
325 correspondence between the internal Visante AS-OCT caliper and the software Straight-line TL  
326 measurements. The thickness measurements obtained are unaffected by the aforementioned  
327 alignment issues because all the ciliary muscle lenses were of constant thickness.

328 The agreement between the ciliary muscle lens thickness values measured by the software and  
329 Vernier calipers demonstrates the software can appropriately compensate for tiered refractive index  
330 levels and the geometric distortion of the exported image in raw DICOM form is negligible. These  
331 findings also support the conclusions of Kao *et al.* [16], who reported images exported from the  
332 Visante AS-OCT images are free from geometric distortions and only need to be adjusted for the  
333 refractive index of the tissue(s) to be suitable for accurate morphological assessment.

334 The bias and variance of the difference in ciliary muscle parameters extracted from 10 patients on 2  
335 separate visits was similar to internal Visante AS-OCT caliper measurement values reported  
336 previously [1]. Furthermore, the limits of agreement reported by the software (-0.166 to 0.135 mm)  
337 were narrower than for the calipers (-0.228 to 0.193 mm) for the measurement of total straight-line  
338 length, suggesting superior repeatability of the localisation of the posterior visible limit by the

339 software. The intersession repeatability of the software developed by Kao and colleagues [16] was  
340 not reported.

341 It is unlikely fully-automated software could be developed to analyse the current ciliary muscle  
342 images produced by the Visante AS-OCT due to the non-uniformity of the acquired image. A custom-  
343 made OCT instrument has been able to obtain sharper definition around the inner apex of the ciliary  
344 muscle, however manual selection of key landmarks is still required to initiate image analysis [21].

345 The newly developed software described by the current study extracts valid and repeatable ciliary  
346 muscle parameters and serves to reduce the subjectivity of ciliary muscle analysis. The image  
347 examiner must be highly trained to extract repeatable results due to the ambiguity of ciliary muscle  
348 landmarks in some patients. The software described here also has the capacity to extract a variety of  
349 additional measurements to previous software [16], including ciliary muscle length, which is a vital  
350 measurement for presbyopia research [16].

## 351 **References**

- 352 [1] Sheppard AL, Davies LN. In vivo analysis of ciliary muscle morphologic changes with  
353 accommodation and axial ametropia. *Invest Ophthalmol Vis Sci.* 2010; 51: 6882-9
- 354 [2] Lewis HA, Kai C, Sinnott LT, Bailey MD. Changes in ciliary muscle thickness during  
355 accommodation in children. *Optom Vis Sci.* 2012; 89(5): 727-37
- 356 [3] Lossing LA, Sinnott LT, Kai C, Richdale K, Bailey MD. Measuring changes in ciliary muscle  
357 thickness with accommodation in young adults. *Optom Vis Sci.* 2012; 89(5): 719-26
- 358 [4] Sheppard AL, Davies LN. The effect of ageing on in vivo human ciliary muscle morphology and  
359 contractility. *Invest Ophthalmol Vis Sci.* 2011; 52: 1809-16
- 360 [5] Richdale K, Sinnott LT, Bullimore MA, Wassenaar PA, Schmalbrock P, Kao CY *et al.* Quantification  
361 of age-related and per diopter accommodative changes of the lens and ciliary muscle in the  
362 emmetropic human eye. *Invest Ophthalmol Vis Sci.* 2013; 54(2): 1095-105

- 363 [6] Bailey MD, Sinnott LT, Mutti DO. Ciliary Body Thickness and Refractive Error in Children. Invest  
364 Ophthalmol Vis Sci. 2008; 49: 4352-60
- 365 [7] Jeon S, Lee WK, Lee K, Moon NJ. Diminished ciliary muscle movement on accommodation in  
366 myopia. Exp Eye Res. 2012; 105: 9-14
- 367 [8] Buckhurst H, Gilmartin B, Cubbidge RP, Nagra M, Logan NS. Ocular biometric correlates of ciliary  
368 muscle thickness in human myopia. Ophthalmol Physiol Opt. 2013;33(3):294-304
- 369 [9] Pucker AD, Sinnott LT, Kao C, Bailey MD. Region specific relationships between refractive error  
370 and ciliary muscle thickness in children. Invest Ophthalmol Vis Sci. 2013; 54: 4710-6
- 371 [10] Oliveira C, Tello C, Liebmann JM, Ritch R. Ciliary body thickness increases with increasing axial  
372 myopia. Am J Ophthalmol. 2005; 140(2): 324-5
- 373 [11] Muftuoglu O, Hosal BM, Zilelioglu G. Ciliary body thickness in unilateral high axial myopia. Eye.  
374 2009; 23(5): 1176-81
- 375 [12] Jeon S, Lee WK, Lee K, Moon NJ. Diminished ciliary muscle movement on accommodation in  
376 myopia. Exp Eye Res. 2012; 105: 9-14
- 377 [13] Dada T, Sihota R, Gadia R, Aggarwal A, Mandal S, Gupta V. Comparison of anterior segment  
378 optical coherence tomography and ultrasound biomicroscopy for assessment of the anterior  
379 segment. J Cataract Refract Surg. 2007; 33: 837-40
- 380 [14] Dirckx JJ, Kuypers LC, Decraemer WF. Refractive index of tissue measured with confocal  
381 microscopy. J Biomed Opt. 2005; 10(4): 0440141-0440148
- 382 [15] Tearney GJ, Brezinski ME, Southern JF, Bouma BE, Hee MR, Fujimoto JG. Determination of the  
383 refractive index of highly scattering human tissue by optical coherence tomography. Opt Lett.  
384 1995; 20: 2258-61
- 385 [16] Kao CY, Richdale K, Sinnott LT, Grillott LE, Bailey MD. Semiautomatic extraction algorithm for  
386 images of the ciliary muscle. Optom Vis Sci. 2011; 88: 275-89
- 387 [17] Bailey MD. Letter: How should we measure the ciliary muscle? Invest Ophthalmol Vis Sci. 2011;  
388 52: 1817-8

389 [18] Sakata LM, Lavanya R, Friedman DS, Aung HT, Seah SK, Foster PH et al. Assessment of the scleral  
390 spur in anterior segment optical coherence tomography images. Arch Ophthalmol. 2008; 126(2):  
391 181-5

392 [19] Richdale K, Bullimore MA, Zadnik K. Lens thickness with age and accommodation by optical  
393 coherence tomography. Ophthal Physiol Opt. 2008; 28: 441-7

394 [20] Bland JM, Altman DG. Statistical methods for assessing the agreement between two methods of  
395 clinical measurement. Lancet. 1986; 327(8476): 307-10

396 [21] Ruggeri M, Hernandez V, Freitas C, Manns F, Parel JM. Biometry of the ciliary muscle during  
397 dynamic accommodation assessed with OCT. Proc SPIE 8930, Ophthalmic Technologies XXIV,  
398 89300W. 2014; doi: 10.1117/12.2044309

399

400 **Table 1.** Comparison of parameters obtained from 5 artificial ciliary muscle sections by the software  
401 and Vernier calipers. A negative mean difference indicates the software values are larger than the  
402 Vernier caliper measurements.

| Parameter      | Mean<br>difference<br>(mm) | Standard<br>deviation<br>(mm) | Limits of agreement |       | t      | p     |
|----------------|----------------------------|-------------------------------|---------------------|-------|--------|-------|
|                |                            |                               | Lower               | Upper |        |       |
|                |                            |                               | (mm)                | (mm)  |        |       |
| Total diameter | 0.046                      | 0.092                         | -0.135              | 0.226 | 3.507  | 0.001 |
| CM25           | -0.001                     | 0.017                         | -0.034              | 0.032 | -0.427 | 0.671 |
| CM50           | -0.003                     | 0.016                         | -0.034              | 0.028 | -1.458 | 0.151 |
| CM75           | 0.000                      | 0.016                         | -0.031              | 0.031 | -1.810 | 0.857 |

403

404

405 **Table 2.** Comparison of ciliary muscle parameters obtained from 50 patients by the software and  
 406 the internal Visante AS-OCT calipers. A negative mean difference indicates the software values are  
 407 larger than the caliper measurements.

| Parameter        | Mean       | Standard  | Limits of agreement |       | <i>t</i> | <i>p</i> |
|------------------|------------|-----------|---------------------|-------|----------|----------|
|                  | difference | deviation | Lower               | Upper |          |          |
|                  | (mm)       | (mm)      | (mm)                | (mm)  |          |          |
| Straight-line TL | 0.011      | 0.089     | -0.163              | 0.185 | 0.860    | 0.394    |
| Max T            | -0.005     | 0.043     | -0.089              | 0.079 | -0.864   | 0.392    |

408  
 409  
 410  
 411  
 412  
 413  
 414  
 415  
 416  
 417  
 418  
 419  
 420  
 421  
 422

423 **Table 3.** Intersession repeatability data of ciliary muscle parameters extracted by the software from  
 424 2 visits of 10 patients. A negative mean difference indicates the measurement was larger at visit 1.

| Parameter        | Mean<br>difference<br>(mm) | Standard<br>deviation<br>(mm) | Limits of agreement |       | t      | p     |
|------------------|----------------------------|-------------------------------|---------------------|-------|--------|-------|
|                  |                            |                               | Lower               | Upper |        |       |
|                  |                            |                               | (mm)                | (mm)  |        |       |
| Straight-line TL | -0.016                     | 0.077                         | -0.166              | 0.135 | -0.569 | 0.583 |
| Curved TL        | -0.017                     | 0.072                         | -0.157              | 0.124 | -0.736 | 0.480 |
| Max T            | -0.003                     | 0.022                         | -0.047              | 0.040 | -0.281 | 0.785 |
| Ant L            | 0.011                      | 0.059                         | -0.104              | 0.126 | 0.577  | 0.578 |
| SS-IA            | 0.007                      | 0.054                         | -0.099              | 0.112 | 0.354  | 0.731 |
| CM2              | -0.007                     | 0.030                         | -0.066              | 0.051 | -0.761 | 0.466 |
| CM25             | -0.003                     | 0.018                         | -0.038              | 0.033 | -0.832 | 0.427 |
| CM50             | 0.004                      | 0.023                         | -0.041              | 0.050 | 0.535  | 0.606 |
| CM75             | 0.009                      | 0.020                         | -0.030              | 0.048 | 1.335  | 0.215 |

425  
 426  
 427  
 428  
 429  
 430  
 431  
 432

433 **Table 4.** Ciliary muscle parameters extracted by the software from 10 images acquired from one  
434 patient who removed and repositioned their head between acquisitions.

435

| 436 | Parameter        | Mean (mm) | Standard deviation<br>(mm) |
|-----|------------------|-----------|----------------------------|
| 437 | Straight-line TL | 5.164     | 0.068                      |
| 438 | Curved TL        | 5.228     | 0.075                      |
| 439 | Max T            | 0.482     | 0.014                      |
| 440 | Ant L            | 1.182     | 0.043                      |
| 441 | SS-IA            | 1.254     | 0.052                      |
| 442 | CM2              | 0.345     | 0.025                      |
| 443 | CM25             | 0.475     | 0.016                      |
| 444 | CM50             | 0.261     | 0.015                      |
|     | CM75             | 0.114     | 0.015                      |

445

446

447

448

449

450

451

452

453

455 **Table 5.** Ciliary muscle parameters extracted by the software from one image analysed 10 times.

| <b>Parameter</b> | <b>Mean (mm)</b> | <b>Standard deviation<br/>(mm)</b> |
|------------------|------------------|------------------------------------|
| Straight-line TL | 5.153            | 0.043                              |
| Curved TL        | 5.218            | 0.038                              |
| Max T            | 0.454            | 0.011                              |
| Ant L            | 1.237            | 0.021                              |
| SS-IA            | 1.276            | 0.040                              |
| CM2              | 0.334            | 0.016                              |
| CM25             | 0.456            | 0.008                              |
| CM50             | 0.259            | 0.006                              |
| CM75             | 0.121            | 0.011                              |